Modelling the Fluorescence Quantum Yields of Aromatic Compounds: Benchmarking the Machinery to Compute Intersystem Crossing Rates

*Koen Veys[(1)], Manon H.E. Bousquet[(2)], Denis Jacquemin[(2,3)], and Daniel Escudero[(1)]**

(1) Department of Chemistry, KU Leuven, B-3001 Leuven, Belgium.

(2) Nantes Université, CNRS, CEISAM UMR 6230, F-44000 Nantes, France.

(3) Institut Universitaire de France (IUF), F-75005 Paris, France.

ABSTRACT

The *from-first-principles* calculation of fluorescence quantum yields (FQYs) and lifetimes of organic dyes remains very challenging. In this manuscript we extensively test the static machinery to calculate FQYs. Specifically, we perform an extensive analysis on the parameters influencing the intersystem crossing (ISC), internal conversion (IC), and fluorescence rates calculations. The impact of *i*) the electronic structure (chosen exchange-correlation functional and spin-orbit Hamiltonian), *ii*) the vibronic parameters (coordinate system, broadening function, and dipole expansion), and *iii*) the excited-state kinetic models, are systematically assessed for a series of seven rigid aromatic molecules. Our studies provide more insights into the choice of parameters and the expected accuracy for the computational protocols aiming to deliver FQYs values. Some challenges are highlighted, such as, on the one hand, the difficulty to benchmark against the experimental non-radiative rates, for which the separation between the IC and ISC contributions is often not provided in the literature and, on the other hand, the need to go beyond the harmonic approximation for the calculation of the IC rates.

1. Introduction

One of the key quantities to control and optimize in both photophysical and photochemical applications, ranging from organic light emitting diodes (OLEDs) to organic solar cells, and all kinds of emissive sensors, is the photoluminescence quantum yield, that quantifies the efficiency of a luminescence process. When considering emission from singlet states only, the fluorescence quantum yield (FQY) is often defined as,

$$\mathrm{FQY} = \frac{k_\mathrm{r}}{k_\mathrm{r} + \sum k_\mathrm{nr}}, \tag{1}$$

where k_r is the radiative (or fluorescence) rate, and $\sum k_\mathrm{nr}$ is the sum of all rates leading to the non-radiative decay. According to Kasha's and Kasha-Vavilov's rules, fluorescence takes place from the lowest singlet excited state (S_1) and the FQY is independent of the excitation wavelength.[1,2] The accurate calculation of the FQY and the underlying decay rates would be very helpful for developing and designing new chromophores with tailored properties. Early attempts to predict excited state decay rates relied on empirical formulas like the Strickler-Berg equation[3] for fluorescence rates and the so-called energy gap law for internal conversion (IC) and intersystem crossing (ISC) processes.[4] However, these formulas do not explicitly consider the vibronic coupling between the electronic states and thus, they are not well suited for accurate calculations, especially for the non-radiative decay rates. More recently, machine learning models were used to predict FQYs, although the results remain very dependent on the learning set and do not provide insight into the underlying decay pathways.[5] Among other possible approaches to calculate FQYs we here highlight the recently developed Radiative Surface Hopping method, which enables modeling fluorescence within a semi-classical non-adiabatic molecular dynamics framework.[6] An alternative approach consists of calculating the excited state decay rates in a "static" way using

vibronic calculations and Fermi's golden rule (FGR)-based expressions for fluorescence, IC, and ISC. Once an appropriate excited state kinetic model is chosen, a kinetic master equation can be derived which can be used to obtain the FQY values. This static approach relies on calculating the rate between two states using a multidimensional oscillator model and it requires to input the coordinates and Hessian matrices of the optimized minima, along with the couplings between the states. All these are available from, *e.g.*, time-dependent density functional theory (TD-DFT) calculations. Furthermore, rate calculations can be performed in a fast and efficient way by Fourier transforming the sum-over-vibrational states in the original FGR expression into the time domain. Multiple names and flavors have been used to denote this approach, including the path-integral,[7] thermal vibration correlation function (TVCF)[8] or time-dependent (TD) formalism,[9] here we refer to it as TVCF. This static approach is a very promising screening method for the development of new fluorophores, and it is therefore increasingly popular in the theoretical/computational photochemistry community.[10–12] Despite its successes, its accuracy remains to be fully established since only a few works effectively calculate FQYs for a large and diverse set of molecules and/or consider extensively the computational parameters involved in these calculations.

In this framework, Ou, Peng, and Shuai calculated the FQYs of 13 BODIPY derivatives by combining the fluorescence and IC rate obtained from the TVCF formalism, together, in some cases, with IC rates obtained by an Arrhenius-type decay equation to take into account an accessible conical intersection.[13] This work showed excellent correlation with experiment but did not assess the impact of different parameters such as the inclusion of Duschinsky rotation effects (DRE) or the dependency on the broadening width. These effects were studied by Humeniuk *et al*. for the IC rate using a series of coumarin dyes, allowing these authors to formulate some very useful rules-of-thumb for analyzing results.[14] More recently Manian *et al*. benchmarked many

functionals and parameters on the S_1-S_0 IC rate of perylene.[15] By varying the basis set and exchange correlation functionals (XCFs) for the calculation of the non-adiabatic coupling and Hessian, they obtained an impressive set of data showing large IC rate variations. Thereby, they showed that even for rigid molecules, care should be taken as the results can significantly depend on methodological details. However, this work did not consider the ISC decay pathway, which is experimentally proven to be the main non-radiative decay path in perylene.[16] Therefore, there is still need for a rigorous benchmark which considers not only electronic states of different multiplicity but also assesses the impact of the quantum chemical and vibronic parts of the rate calculations for a significant set of molecules. In this framework, we recently systematically benchmarked many electronic structure levels and vibronic parameters for the calculation of the radiative rate of a series of substituted phenyl derivatives.[17] In the present work, we want to extend this benchmark to the calculation of FQY values. We believe these works therefore contribute to complement other benchmarks and to obtain a better understanding of the expected accuracy of state-of-the-art "static" schemes for determining the FQY values.

One difficulty arises when benchmarking against experimental results, which is the experimental uncertainty itself. The experimental FQYs are available for many organic systems in different solvents but often the data are found to be spread over different works across the literature where different experimental setups and conditions were used. In this regard, systematic experimental works on a large set of fluorophores using a common experimental setup, such as the ones from Berlman[18] and Birks[19] are very helpful to provide curated data for benchmarking purposes. After photon absorption, there are two possible deactivation pathways: radiative and nonradiative. Both the radiative and total non-radiative rates can be experimentally deduced from lifetime measurements and the FQYs. Sometimes, an attempt is made to separate the contributions to the

non-radiative rate into IC and ISC rates, but this is often based on empirical formulas or by completely neglecting one of the two contributions.[16,20] To estimate ISC rates, one can determine the triplet quantum yields by measuring the formation of a triplet quencher, reacting with the T_1 state of the fluorophore. However, the S_1 state of the fluorophore can get significantly quenched as well, hereby influencing the measured yield. To instead determine the rate without influence of the acceptor, the method from Medinger and Wilkinson can be used:[21] they proposed to correct the influence of the quencher by measuring triplet-triplet absorption bands, with and without a triplet quencher. However, the accuracy and applicability of this approach still depends on the assignment of the absorption maxima, the T_1 lifetime, and the absence or presence of reverse ISC. A more accurate separation of rates can be obtained by optoacoustic experiments, where the fast heat dissipation in IC is measured as a sound wave.[22] Unfortunately, this setup remains uncommon, so no systematic measurements on a large set of molecules are available to our knowledge. Thus, we focus the experimental comparison on the fluorescence rates and FQYs.

Seven molecules have been selected in this benchmark, shown in Scheme 1, having FQYs ranging from 10% to almost 100%. In order to maximize the efficiency of the used multidimensional oscillator model, small and rigid molecules were chosen, for which reliable measurements are available and which are not very sensitive to solvents. Table 1 summarizes their photophysical properties, where some deviations are observed due to different experimental conditions. Apart from the FQY values, the radiative rates are also reported, from which the total non-radiative rates are derived.

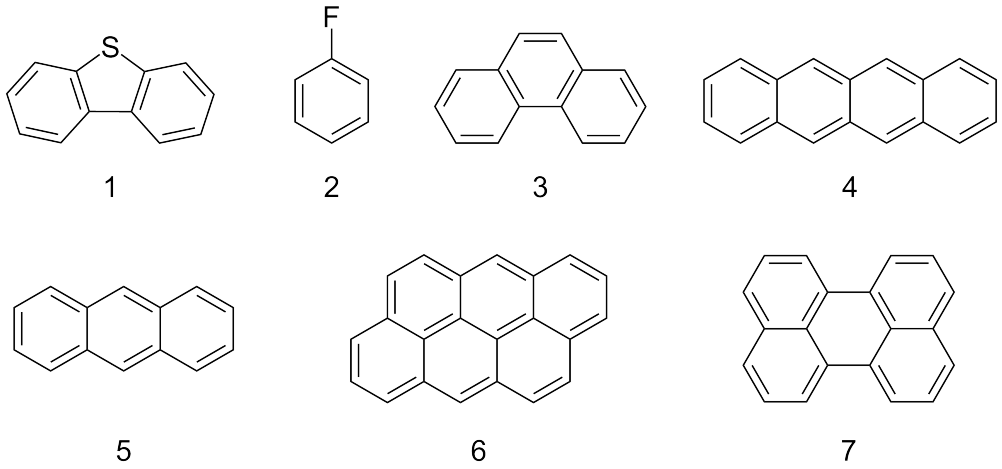

*Scheme 1. Chemical structures of the molecules considered in this work. **1**: dibenzothiophene, **2**: fluorobenzene, **3**: phenanthrene, **4**: tetracene, **5**: anthracene, **6**: anthanthrene, **7**: perylene.*

Table 1. Experimental FQYs and fluorescence rates. The slight variance in FQY and k_r is due to measurements in different solvents and originating from different experiments. The total non-radiative rate is calculated as $k_{nr} = k_r(\frac{1}{FQY} - 1)$.

	Molecule	FQY (unity)	Average FQY	$k_{\mathrm{r}}(10^7\ \mathrm{s}^{-1})$	$k_{\mathrm{nr}}(10^7\ \mathrm{s}^{-1})$	Ref.
1	dibenzothiophene	0.09[a]	0.09	1.4 - 2.9	15 – 30	18
2	fluorobenzene	0.13[a]	0.13	0.27 - 1.8	1.8 – 12	18,19,40
3	phenanthrene	0.10[b] - 0.24[a]	0.17	3.2	10 – 29	18,19,40
4	tetracene	0.16[a,c] - 0.21[a]	0.19	6.3 - 7.7	24 – 40	19,20,40
5	anthracene	0.22[b] - 0.36[a]	0.29	3.3 - 3.7	5.8 – 13	18–20,40
6	anthanthrene	0.73[c]	0.73	15 - 20	5.4 – 7.4	18,40
7	perylene	0.87[b,c] - 0.98[a]	0.93	16	0.32 – 2.4	18,19,40

[a]cyclohexane; [b]ethanol; [c]benzene

2. Theoretical background

2.1. Fluorescence Quantum Yields (FQYs)

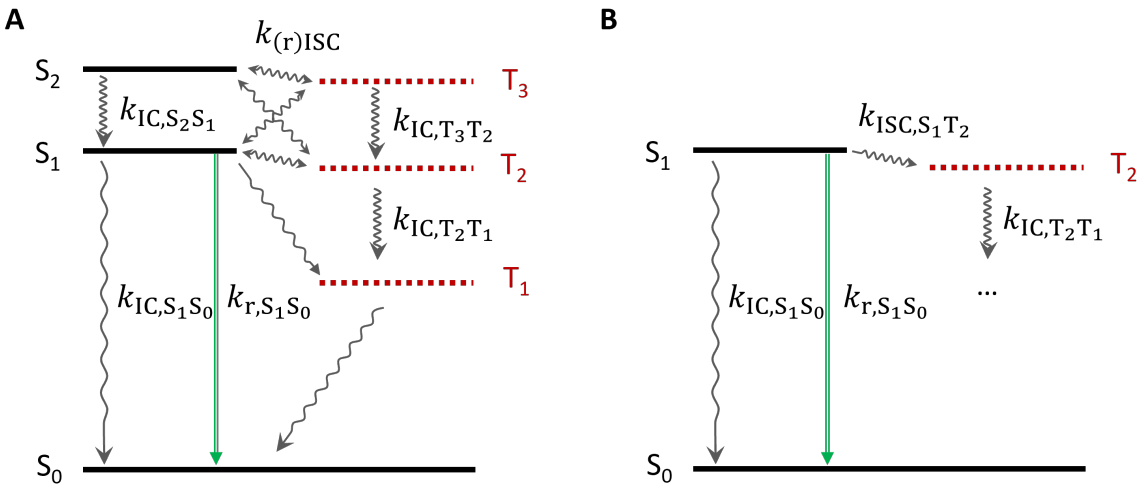

Scheme 2. Full (A) and approximated (B) excited state kinetic models used to calculate the FQY values. Abbreviations: r, radiative; IC, internal conversion; ISC, intersystem crossing; rISC, reverse ISC. Full lines represent singlet (S) states and dotted lines triplet (T) states.

The calculation of FQYs *from-first-principles* requires first an appropriate excited state description and kinetic model, whereafter all possible excited state decay channels can be calculated. For Kasha's-like fluorescence from the S_1 state, one should in principle include in the model all possible decay channels arising from S_1 (see *e.g.*, in Scheme 2A an IC and a radiative channel to S_0 and three different ISC channels to $T_{1\text{-}3}$). For the rigid organic molecules under investigation, the excited state kinetic model represented in Scheme 2A is the most general and complete one, because both T_2 and T_3 states are energetically close to S_1, and concomitantly S_2 is close-lying to T_3 for **1**-**7**, see in Figure S1 in the Supporting Information (SI) for the energetic alignment of the states. Therefore, all IC, ISC, and rISC rates between the latter states should in principle be considered. Under these circumstances, the most accurate approach to calculate the FQYs is by simulating how the population changes over time, by considering all decay channels and numerically solving the associated differential equations, as explained in Section S10 in the SI. To alleviate the computational burden, we have tested simplified excited state kinetic models. Specifically, for the investigated molecular systems here, there are some experimental evidences

that $S_1 \rightarrow T_2$ ISC (in a major extent) and $S_1 \rightarrow S_0$ IC (in a minor extent for some molecular systems only, *e.g.*, **4**) are the main nonradiative decay channels from S_1.[16,21,23] This yields a much simpler kinetic model, as shown in Scheme 2B, where we can neglect transitions involving T_3 and S_2 and also the reverse $T_2 \rightarrow S_1$ ISC. Accordingly, the FQY values for this simplified model are obtained with:

$$\mathrm{FQY} = \frac{k_{\mathrm{r,S_1S_0}}}{k_{\mathrm{r,S_1S_0}} + k_{\mathrm{ISC,S_1T_2}} \; (+k_{\mathrm{IC,S_1S_0}})} \qquad (2)$$

where k_{IC,S_1S_0} is of minor relevance for **1**-**7**. Naturally, this approximate model is not necessarily generally valid. In Section 4.1, we validate Eq. (2) for **1**-**7** by comparing it with the full kinetic simulations, including all possible decay rates.

2.2. Excited State Decay Rates

Once the kinetic model to calculate FQYs is chosen, the next step is to calculate the excited state decay rates themselves. The transition rates between the involved electronic states are given by their corresponding FGR expressions in which an appropriate perturbation is applied (*vide infra*).[24]

In practice, the computational procedure to evaluate rates consists of three steps: i) geometry optimization and frequency calculation for the two involved electronic states; ii) selection of a specific vibronic model (coordinates, potential energy surface model) and application (or not) of the Duschinsky rotation effects; and iii) the computation of the rates themselves. There are two choices for the last step: through the evaluation of a theoretically infinite sum over vibrational states, the so-called time-independent (TI) approach, or through the evaluation of an integral involving the Fourier transformed vibrational states (the TD or TVCF approach).[8,14,25] The TVCF formalism has been extensively discussed in the literature, and we refer the readers to Refs. [14], [25] and [26] for more information. While the first step can be performed with any quantum

chemistry program, the latter is only implemented in a handful of codes, including FCClasses[27], ORCA[28], and MOMAP[29].

2.2.1. FGR and vibronic models

The rate (k_{if}), between two electronic states (i, f) is given by FGR according to:[24]

$$k_{if} = \frac{2\pi}{\hbar} \left| \langle \Psi_f | \hat{\mathcal{H}}' | \Psi_i \rangle \right|^2 \rho \tag{3}$$

where ρ is the density of states and $\langle \Psi_f | \hat{\mathcal{H}}' | \Psi_i \rangle$ the perturbation matrix between the states. The total wavefunction (Ψ) can be approximated by the product of its electronic (Φ) and vibrational (Θ) parts following the Born-Oppenheimer approximation,

$$k_{if} = \frac{2\pi}{\hbar} \sum_{\nu,\nu'} \left| \langle \Phi_{\mathrm{f}} \Theta_{f,\nu'} | \hat{\mathcal{H}}' | \Phi_i \Theta_{i,\nu} \rangle \right|^2 \rho \tag{4}$$

where we sum over the initial (ν) and final (ν') vibrational wavefunctions. Many rates can be derived from this expression, but in this work, we will focus on the fluorescence, IC, and ISC rates. The former is obtained when using the dipole operator as a perturbation, while the IC rate is determined when using the nonadiabatic coupling (NAC) operator instead. Finally, using the spin-orbit coupling (SOC) operator provides the ISC rate.

An important step in each of these calculations is the computation of the overlap between the vibrational wavefunctions of the two involved electronic states. Different vibronic models relying on the multidimensional harmonic oscillator approximation[14] are available, of which the adiabatic Hessian (AH), vertical Hessian (VH) and vertical gradient (VG) are probably the most used. AH can be viewed as the most refined vibronic model, though it will fail if the two states have too different geometries. In this work, given that we have (very) rigid compounds, all calculations use the AH approximation, where the vibrational wavefunctions are represented by a multidimensional harmonic oscillator at the minima of their respective electronic states.[14] The normal modes of one

of the states are then rotated and translated to the frame of reference of the other state (Duschinsky rotation). Besides being dependent on the used vibronic model, the rate calculations also depend on several parameters including the finite broadening, the coordinate system (Cartesian or internal), the inclusion or not of Herzberg-Teller effects, etc. In this contribution we assess the impact of these parameters on the fluorescence, IC, and ISC rate calculations, which are shortly described below.

2.2.2. Fluorescence

Using as perturbation the electric dipole operator ($\vec{\mu}$) in Eq. (3) and applying it to the electronic part of the wavefunction, one obtains the emission spectrum (σ_{em}):[8]

$$\sigma_{\text{em}}(\omega) = \frac{2\omega^3}{3\pi\hbar c^3} \sum_{\nu,\nu'} P_{i,\nu}(T) \left| \langle \Theta_{f,\nu'} | \vec{\mu}_{if} | \Theta_{i,\nu} \rangle \right|^2 \delta\left(E_{if} + E_{i\nu} - E_{f\nu'} - \hbar\omega\right) \tag{5}$$

where $\vec{\mu}_{if}$ is the electric transition dipole operator, $P_{i,\nu_i}(T)$ is the Boltzmann distribution for the initial state, ω is the emission energy, c is the speed of light, $\hbar$ is the reduced Planck's constant, and δ is the Dirac delta function which selects the energy corresponding to the transition. $\vec{\mu}_{if}$ depends on the nuclear coordinates (Q_k) and it can be expanded as:

$$\vec{\mu}_{if}(Q_k) = \vec{\mu}_0 + \sum_k \left(\frac{\partial \vec{\mu}_{if}}{\partial Q_k} \right)_0 Q_k \tag{6}$$

where $\vec{\mu}_0$ is the zeroth-order electric transition dipole moment (TDM) in the Franck-Condon (FC) approximation, and the second term refers to the so-called Herzberg-Teller (HT) effects.

Re-casting Eq. (6) into the time-domain and applying the FC approximation gives:[8,9]

$$\sigma_{\text{em}}(\omega) = \frac{2\omega^3}{3\pi\hbar c^3} |\vec{\mu}_0| \int_{-\infty}^{\infty} e^{-i(\omega-\omega_{if})t} * Z_{iv}^{-1} * \chi_{\text{fluo}}(t,T) * g(t)\, dt \tag{7}$$

where $\chi_{\text{fluo}}(t,T)$ is the correlation function for fluorescence, Z_{iv}^{-1} is the partition function coming from the Boltzmann distribution, and $g(t)$ is the broadening function. For the sake of

completeness, we point out that Cerezo and Santoro[9] used the name TDM correlation function for $|\vec{\mu}_0|Z_{iv}^{-1}\chi_{\text{fluo}}(t,T)$, while Niu *et al.*[8] combined the product of $\chi_{\text{fluo}}(t,T)$ and $g(t)$ as the TVCF. Finally, the radiative rate can be obtained by integrating over the emission spectrum:

$$k_{\text{r}} = \int_0^\infty \sigma_{\text{em}}(\omega)d\omega \tag{8}$$

By considering the first two terms in Eq. (6) one can derive the HT-corrected expression for the emission spectrum, see details in Ref. [8]. For weakly allowed transitions, the HT terms can be predominant.[30–32]

2.2.3. Internal Conversion

Using the NAC operator as the perturbation operator and inserting it in Eq. (3) yields the IC rate:[8,9]

$$k_{\text{ic}} = \sum_{k,l} \frac{R_{kl}}{\hbar^2} \int_{-\infty}^{\infty} e^{i\omega_{if}t} * Z_{iv}^{-1} * \chi_{\text{ic}}(t,T) * g(t)\, dt \tag{9}$$

where $\chi_{\text{ic}}(t,T)$ is the correlation function for IC, and R_{kl} is the electronic part of the NAC, which after applying the Condon approximation can be taken out of the integration.[8] Just like the TDM, the NAC can be obtained from quantum chemical calculations. However, although a derivation of an HT-like expansion for the IC rate exists,[33] it is not widely implemented in the available codes devoted to rate calculations, and the impact of HT effects on IC rates remains to be established.

2.2.4. Intersystem crossing

In a first approximation, the SOC operator ($\widehat{\mathcal{H}}_{\text{SO}}$) does not depend on the nuclear coordinates, which makes it possible to simplify Eq. (3) for the ISC rate as:[34]

$$k_{\text{isc}} = \frac{2\pi}{\hbar} \left|\left\langle \Phi_{\text{S}_i} \middle| \widehat{\mathcal{H}}_{\text{SO}} \middle| \Phi_{\text{T}_f} \right\rangle\right|^2 \sum_{v,v'} P_{i,v_i}(T) \left|\langle v_i | v_f \rangle\right|^2 \delta\left(E_{if} + E_{iv} - E_{fv'} - \hbar\omega\right) \tag{10}$$

After Fourier transformation, Eq. (10) can be rewritten in a TD variant, see Ref. [34] for details. For most molecules with heavy atoms and significantly large electronic SOC matrix elements (from ~10 cm^{-1}) between the involved electronic states, Eq. (10) provides rather accurate results.[35,36] However, many organic molecules presenting negligible electronic SOCs still show significant ISC.[34] In these cases, the ISC is driven by the coupling of electronic SOCs with the vibrational degrees of freedom. Analogously to fluorescence, an HT-like expression also exists for ISC and has been implemented in dedicated codes for excited state rate calculations.[28,37] In the latter expression, the electronic SOC operator additionally includes the first-order term of the tailor expansion in Q_k, *i.e.*, the vibronic spin-orbit interaction:[34]

$$\mathrm{SOC}(Q_k) = \left(\left\langle \Psi_{\mathrm{S}_i} \middle| \widehat{\mathcal{H}}_{\mathrm{SO}} \middle| \Psi_{\mathrm{T}_f} \right\rangle\right)_0 + \sum_k \left(\frac{\partial \left\langle \Psi_{\mathrm{S}_i} \middle| \widehat{\mathcal{H}}_{\mathrm{SO}} \middle| \Psi_{\mathrm{T}_f} \right\rangle}{\partial Q_k} \right)_0 Q_k \qquad (11)$$

To the best of our knowledge, no analytical implementation of this equation is available yet, but instead a finite-difference technique is used to obtain the derivatives of the electronic SOC matrix elements,[36]

$$\left(\frac{\partial \left\langle \Psi_{\mathrm{S}_i} \middle| \widehat{\mathcal{H}}_{\mathrm{SO}} \middle| \Psi_{\mathrm{T}_f} \right\rangle}{\partial Q_k} \right)_0 \approx \frac{\left(\left\langle \Psi_{\mathrm{S}_i} \middle| \widehat{\mathcal{H}}_{\mathrm{SO}} \middle| \Psi_{\mathrm{T}_f} \right\rangle\right)_{0+d} - \left(\left\langle \Psi_{\mathrm{S}_i} \middle| \widehat{\mathcal{H}}_{\mathrm{SO}} \middle| \Psi_{\mathrm{T}_f} \right\rangle\right)_{0-d}}{2d} = \frac{\Delta \mathrm{SOC_k}}{2d} \qquad (12)$$

Within the finite difference approach the chosen displacement (d) and coordinate system can potentially have a non-trifling influence on these derivatives, so care needs to be taken when using this approach. Finally, the underlying approximations of $\widehat{\mathcal{H}}_{\mathrm{SO}}$ are also essential, as summarized below and detailed in other works.[35,38]

2.2.4.1. *Spin-orbit Hamiltonian*

All SOCs and ISC calculations presented here rely on the use of a Breit-Pauli spin-orbit (SO) Hamiltonian, *i.e.*,[35,38]

$$\hat{\mathcal{H}}_{\mathrm{SO}}^{\mathrm{BP}} = \hat{\mathcal{H}}_{\mathrm{SO}}^{\mathrm{BP-1e}} + \hat{\mathcal{H}}_{\mathrm{SO}}^{\mathrm{BP-2e}} \tag{13}$$

with $\hat{\mathcal{H}}_{\mathrm{SO}}^{\mathrm{BP-1e}}$ and $\hat{\mathcal{H}}_{\mathrm{SO}}^{\mathrm{BP-2e}}$ being the one- and two-electron operators:

$$\hat{\mathcal{H}}_{\mathrm{SO}}^{\mathrm{BP-1e}} = \frac{1}{2\mathrm{m_e^2c^2}} \sum_i \sum_I \frac{Z_I}{|\hat{r}_{ij}|^3} (\hat{r}_{iI} \times \hat{p}_i) \cdot \hat{s}_i \tag{14}$$

$$\hat{\mathcal{H}}_{\mathrm{SO}}^{\mathrm{BP-2e}} = \frac{-1}{2\mathrm{m_e^2c^2}} \sum_i \sum_{j \neq i} \frac{1}{|\hat{r}_{ij}|^3} (\hat{r}_{ij} \times \hat{p}_i) \cdot (\hat{s}_i + 2\hat{s}_j) \tag{15}$$

where Z_I is the charge of nucleus I; $\hat{p}$ and $\hat{s}$ are, respectively, the electron momentum and spin operators; $\hat{r}_{iI}$ ($\hat{r}_{ij}$) is the position vector between electron *i* and nucleus *I* (electron *j*); and $\mathrm{m_e}$ and c are the electron mass and speed of light, respectively.

In its most approximated form, the two-electron terms are fully discarded and the nuclear charges are used as a parameter instead, an approach denoted the effective nuclear charge (ENC) approximation.[38] Alternatively, the two-electron terms can be approximated by a spin-orbit mean-field (SOMF) approach resulting in coulombic, exchange, and correlation contributions to the SOCs, similar to how the energy is partitioned in DFT. The approximated or exact calculation of each of the last three terms leads to different schemes to compute SOCs, which are systematically assessed in this work. Neese and coworkers found that using the RI approximation for the coulombic part and one-center integrals[39] for the exchange part leads to results with an error smaller than 10% when comparing to experimental g-tensors.[38] However, a systematic assessment of the different approaches to evaluate the SOC derivatives is lacking. On the one hand, if the SOCs are very small, these calculations might be more prone to numerical errors, whereas on the

other hand, systematic errors in the evaluation of the SOC derivatives might cancel out when using a finite difference approach.

3. Computational details and experimental data

Table 1 collects the experimental data for compounds **1-7**, sorted by increasing FQY. The combination of different experimental setups and solvents results in a variability of the experimental FQY values by ca. 10%. In combination with the error on the experimental fluorescence rates of up to one order of magnitude, this results in a significant spread for the resulting non-radiative rates.

Scheme 3 shows an overview of the computational workflow used in this work. Ground and excited-state geometries were optimized using DFT[41–43] and TD-DFT,[44,45] respectively, using the Tamm-Dancoff approximation (TDA) for the latter[46] in combination with the 6-311G(d,p) atomic basis set. Five different exchange-correlation functionals (B3LYP[47], PBE0[48], M06-2X[49], CAM-B3LYP[50], and ωB97X-D[51]) were used to benchmark the calculation of FQYs. Whenever we do not specify a functional, PBE0 is used.

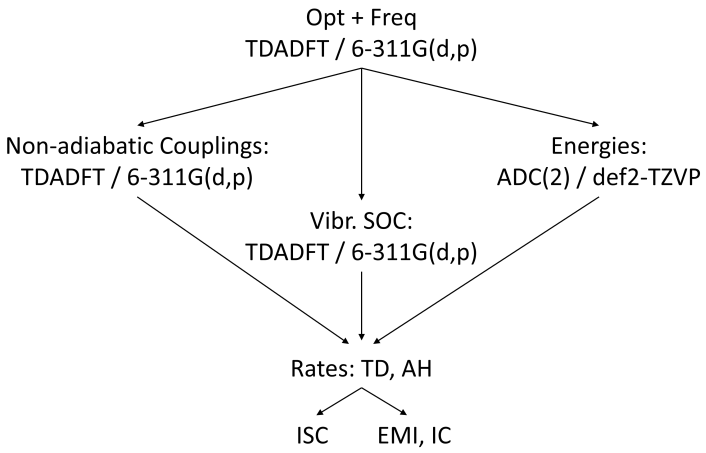

Scheme 3. Schematic overview of the computational workflow. Abbreviations: Opt + Freq is optimization and frequency calculation, EMI is emission. All other abbreviations can be found in the text.

As mentioned above, an appropriate excited state kinetic model accounting for all possible decay channels should be devised (see Scheme 2). To this aim, the geometries of S_1-S_2 and T_1-T_3 for **1**-**7** were optimized. All minima were checked for imaginary frequencies, and only the T_3 state of **1** with CAM-B3LYP showed one imaginary frequency, which was later proven to have no influence on the results (see Section 4.1). All optimizations and frequency calculations were performed with Gaussian version 16A03, using default convergence criteria and grids.[52] Initially, full symmetry was used for each state, and this was lowered when imaginary frequencies were obtained. From these calculations, the transition dipole moment, gradient, and Hessian matrix were used directly for all radiative and IC rate calculations, while they were converted to an ORCA 5.0.3[28] Hessian file format for ISC rate calculations using an in-house script. The same functionals (and basis set) were used to calculate the nonadiabatic couplings in Q-CHEM, version 5.3 (using default parameters and convergence criteria), at the TDA-DFT level using the semi-wavefunction approach with electron-translation factors (ETF) correction.[53,54] This is necessary to obtain NACs between excited states (*e.g.* T_2-T_1), which are not implemented in Gaussian version 16A03.[55] SOCs were calculated at the TDA-DFT level with ORCA 5.0.3.[28,56] A higher DFT integration grid

(*defgrid3*) was specified to obtain accurate SOC derivatives. Unless specified, the spin-orbit mean-field (SOMF) approximation was used, including one-electron terms together with exact Coulomb terms, analytic exchange terms, and local DFT correlation for the two-electron terms.[38] Four-center integrals were used for both coulomb and exchange terms without further approximations, by specifying the "*SOCFlags = 1,4,4,1"* option.

Single point energy calculations were performed on top of each optimized geometry using the second-order algebraic diagrammatic construction (ADC(2)) method.[57] The def2-TZVP basis set[58] was employed for these calculations, in combination with the spin-component-scaled (SCS) approach[59] and the resolution of identity (RI) approximation, but without frozen core approximation. The SCS-ADC(2) calculations were done in Turbomole, version 7.1, with the default parameters.[60]

Finally, we performed three types of rate calculations (fluorescence, IC, and ISC) using the TD method, with the AH model for the vibrations including the DRE.[61] Geometries, gradients, Hessian matrices, TDMs, NACs, and SOCs were obtained from the TDA-DFT calculations detailed above, while energies were taken from the ADC(2) calculations. The temperature was set to 298 K, Cartesian coordinates were used in the vibronic model, and a Lorentzian broadening was applied with a the full-width at half-maximum (FWHM) of 10 cm^{-1} unless specified otherwise. For the radiative rates, the FC+HT TDM model was used. Radiative and IC rates were calculated with FCClasses 3.0.1,[27] while ISC rates were computed with ORCA 5.0.3. For the latter, the Herzberg-Teller-like vibrational SOCs were included, and the obtained rates are the average of the three spin substates (MS) = {+1, 0, -1} contributions.

Solvent effects were excluded in all calculations to avoid having an extra variable. However, the solvent does not significantly affect the FQY values for the chosen molecules, as seen in Table 1, where the latter values only vary slightly in the different solvents used.

4. Results and discussion

We structured the results as follows. First, we validate the excited state kinetic models to calculate the FQYs. Then, the quality of the harmonic approximation is assessed by investigating the influence of the broadening and coordinate system on the computed rates. Next, different computational options for the calculation of fluorescence and intersystem crossing rates are discussed. Finally, the influence of the chosen XCF on the computed FQYs is assessed.

4.1. FQYs: Excited state kinetic models

As discussed above, full (see Scheme 2A) and/or approximated (see Scheme 2B) excited state kinetic models have been devised to calculate the FQYs of **1**-**7**. Three different models are considered herein: *i*) the full kinetic simulation, considering all the rates between $S_{1/2}$ and $T_{1/2/3}$ states; *ii*) the simplified kinetic Eq. (2); and *iii*) a similar equation, including the $S_1 \rightarrow T_3$ ISC pathway:

$$\mathrm{FQY}' = \frac{k_{\mathrm{r},S_1S_0}}{k_{\mathrm{r},S_1S_0} + k_{\mathrm{ISC},S_1T_2} + k_{\mathrm{ISC},S_1T_3}} \tag{16}$$

However, all models neglect the $S_1 \rightarrow S_0$ IC rate, since the energy difference is very large, bringing the calculation outside of the harmonic regime, as discussed in Sections 4.2 and Section 4.5. It is of course still possible to calculate the $S_1 \rightarrow S_0$ IC rates with the usually applied Lorentzian broadening with a FWHM of 10 cm^{-1},[14] keeping in mind its limited meaning. For our systems, the resulting rates from this approach are rather small compared to the fluorescence and ISC rates for most compounds (see Table S2 in the SI).

Table 2 collects the results with the different excited state kinetic models. First, we note that for **1**-**7** the use of Eq. (16) yields exactly the same results as the full kinetic simulations. The inclusion of the S_2 state therefore does not make a difference and can be safely left out. We ascribe these results to the very small reversed ISC, *i.e.*, $\frac{k_{\mathrm{ISC},T_2S_1}}{k_{\mathrm{ISC},T_2T_1}} < 10^{-2}$ in all the investigated cases (See Table S2 for all the excited state decay rates).

We then investigate the effect of including additional decay channels. As shown in Figure S1 and Table S1 in the SI the $S_1 \rightarrow T_3$ ISC channel is thermodynamically uphill for **1**-**7**. Therefore, including this additional ISC channel leads to slight changes in the computed FQYs values only. For **2** and **3** the effect is nevertheless noticeable with a variation of the predicted yield of ca. 2-3%. This variability is within the experimental error and irrelevant for our purposes, so that the most simplified equation (3) is generally used in the following, unless specified otherwise. However, we note that for an arbitrary organic molecule the use of the full simulation might still be more appropriate. We also note that the data of Table 2 are not perfectly fitting experiment, but this aspect is discussed below.

Table 2. Calculated FQY values without (FYQ) and with (FQY') the inclusion of the S_1-T_3 ISC rate, as well as the full simulation considering all the rates between $S_{1/2}$ and $T_{1/2/3}$ states. $FQY = \frac{k_{r,S_1S_0}}{k_{r,S_1S_0}+k_{ISC,S_1T_2}}$; $FQY' = \frac{k_{r,S_1S_0}}{k_{r,S_1S_0}+k_{ISC,S_1T_2}+k_{ISC,S_1T_3}}$. SCS-ADC(2)/def2-TZVP//TDA-PBE0/6-311G(d,p) calculations with the AH, FC+HT, Cartesian vibronic model using a 10 cm^{-1} Lorentzian broadening.

	FQY	FQY'	$Full\ simulation$
1	0.76	0.76	0.76
2	0.61	0.58	0.58
3	0.36	0.34	0.34
4	0.82	0.82	0.82
5	0.82	0.82	0.82
6	0.92	0.92	0.92
7	1.00	1.00	1.00

4.2. Coordinate system and broadening function

As mentioned above, we aim at a systematic exploration of the parameters impacting the computed rates. We here assess the influence of the chosen coordinate system and the broadening width. For the former, while using unambiguous Cartesian coordinates to construct the PES seems attractive, they are often unsuited for molecules with large amplitude motions, such as torsional displacements. In that case, curvilinear internal coordinates should provide much more reliable results. Especially with the VH model (not used here), using Cartesian coordinates to expand the PES at a geometry different from the minimum often yields unphysical imaginary frequencies, an effect tempered by internal coordinates.[62] For the broadening, the Dirac δ function which selects the energy difference is replaced with a broadening function during the Fourier transform in the TD model. This function can be a Gaussian, a Lorentzian, or a combination of both, that is a Voigtian function.[14]

For the analyses below we perform pair-wise comparisons to estimate the influence of a given parameter, *i.e.*, we only change the coordinate system while keeping the rest of parameters unchanged. However, we refrain ourselves from doing a statistical analysis because of the limited set of molecules investigated.

Both parameters give important insights into the validity of the vibronic calculations and therefore the quality of the computed rates. For instance, when Cartesian and internal coordinates yield the same rates, it indicates that the Duschinsky rotation effect is accurately described.[63] If the magnitudes of the non-radiate rates are dominated by FWHM of the Lorentzian broadening it indicates that the harmonic approximation is not valid, and that the broadening is responsible for the non-radiative rate.[14] Figure 1 and Table S3 in the SI show the differences obtained for the fluorescence and ISC rates when changing the coordinate system used to construct the vibrational

space. We recall that our calculations rely on the AH model, and therefore, both coordinate systems should behave identically would the harmonic approximation be valid. For the radiative rates, and in agreement with previous investigations,[17] the selection of the coordinate system has a small influence on the computed rates. For **1**-**7**, slightly smaller k_r values are obtained when using internal coordinates. A maximum absolute difference of 11% (for **2**) is obtained between the two approaches, which is rather small, as the rates vary over several orders of magnitude. For the ISC rate, we here focus on the predominant ISC channel determining the FQYs, *i.e.*, the $S_1 \rightarrow T_2$ channel. Overall, slightly larger k_{ISC} values are obtained when using internal coordinates rather than their Cartesian counterparts, but the variability between the two approaches remains acceptable. A maximum absolute deviation of 39% is obtained again for the k_{ISC} of **2**. Finally, we note that, generally, for an arbitrary organic molecule, the use of internal coordinates is preferred over the use of Cartesian ones, especially when large amplitude motions are at play.[64] However, since our protocol involves calculations with multiple programs, we stuck to Cartesian coordinates in the following since these can be more easily consistently defined.

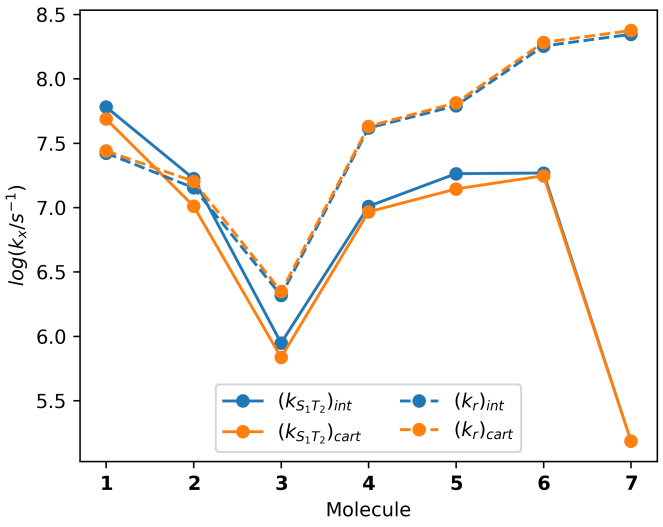

Figure 1. Comparison between cartesian (cart, orange) and internal (int, blue) coordinates for the calculated fluorescence and ISC rates. SCS-ADC(2)/def2-TZVP//TDA-PBE0/6-311G(d,p) calculations with AH, FC+HT vibronic model using a 10 cm^{-1} Lorentzian broadening.

Next, we explore the influence of the chosen broadening on the computed rates. A Lorentzian type of broadening enables reproducing the homogenous broadening. A Gaussian function is best suited to phenomenologically capture the inhomogeneous broadening. Inhomogeneous (Gaussian) broadening functions influence the shape of the computed emission spectra, but have little effect on both the non-radiative and radiative rates.[14] For a Lorentzian broadening, choosing an FWHM in the 1 - 500 cm^{-1} range is found to be almost inconsequential for the radiative rates of **1**-**7** (see Table S4), in full agreement with literature.[14]

Conversely, the IC and ISC rate calculations can be heavily dependent on the chosen FWHM value of the Lorentzian function. In our set, this dependency can be seen in Table 3. When varying the FWHM from 1 to 100 cm^{-1}, the IC rate changes with a factor of 10^2. This is likely an artifact of the calculation, typically happening when the IC rate is rather low, and it clearly raises the question of the validity of the harmonic approximation for the IC calculations of **1**-**7**. We note that the adiabatic energy difference between S_1 and S_0 is ca. 3 eV for all compounds, which likely makes the harmonic approximation invalid for IC rate calculations. Using anharmonically corrected formalisms to calculate the IC rates might be needed to obtain accurate IC rates in **1**-**7**.[65,66] In contrast to the IC rates, the ISC rates for the $S_1 \rightarrow T_2$ channel are less dependent on the chosen FWHM (see Table 3), except for **7**, which has an uphill $S_1 \rightarrow T_2$ decay and thus a rather low k_{ISC}. Under these circumstances, the harmonic approximation holds true for the ISC rate calculations, which can be ascribed to the rigidity of the molecular systems under investigation and to the small adiabatic energy difference between the involved electronic states (< 1 eV). We also note that, regardless of the chosen broadening, the computed ISC rates in Table 3 are generally larger than the IC rates. The available experimental data for **1**-**7** consistently point to ISC-dominated nonradiative decays.[16,21] Under these circumstances, and as

evoked above, our FQY estimations for **1**-**7** obviate the IC contributions (see an exception for **4** in Section 4.5, for which experimental IC and ISC data are available).

Table 3. Logarithm of IC and ISC rates for different FWHM values of the Lorentzian broadening. SCS-ADC(2)/def2-TZVP//TDA-PBE0/6-311G(d,p) calculations using the AH, FC+HT, Cartesian vibronic model.

	$\log(k_{IC,S_1S_0}/s^{-1})$			$\log(k_{ISC,S_1T_2}/s^{-1})$		
FWHM (cm^{-1})	1	10	100	1	10	100
1	5.9	6.9	7.9	6.0	5.8	6.1
2	5.4	6.4	7.4	7.2	7.0	7.3
3	5.6	6.6	7.6	7.8	7.7	7.9
4	5.1	6.1	7.1	7.0	7.0	7.2
5	4.6	5.6	6.6	7.3	7.1	7.3
6	5.0	6.0	7.0	7.3	7.2	7.2
7	4.8	5.8	6.8	4.7	5.2	6.1

All in all, both the coordinate system and the broadening have minor impact on the calculated ISC rates for **1**-**7**. Therefore, Cartesian coordinates and a Lorentzian broadening of 10 cm^{-1} are systematically used in the next sections for the ISC rates.

4.3. Influence of the Spin-Orbit Hamiltonian on the ISC rates

As mentioned above, the $S_1 \rightarrow T_2$ ISC channel provides the largest contribution to the non-radiative decay of **1**-**7**. We note that all these ISC rates are 100% obtained from the HT contribution, *e.g.*, the second term in Eq. (11), so that the FC expression for ISC is simply not appropriate for these molecular systems.

We now turn to an investigation of the influence of the chosen Breit-Pauli SO Hamiltonian for the SOC calculations. Figure 2 collects the results for the computed SOCs and ISC rates for the $S_1 \rightarrow T_2$ channel obtained at different approximations of this Hamiltonian. The numerical results are listed in Tables S4-S5. As discussed above, fully neglecting the two-electron terms, and making

use of the ENC approximation leads to the most approximated approach to calculate SOCs and k_{ISC}. Conversely, one can include the two-electron terms in the SOMF model. Within the SOMF, calculating the two-electron Coulomb, exchange, and correlation terms (without the use of the RI approximation and using four-center integrals) leads in principle to the most accurate SOMF approach, and is considered here as our theoretical best estimate (TBE). A few more approximations, namely the exclusion of correlation (SOMF-NoCor), the use of the RI approximation for the Coulomb terms (SOMF-CouRI) and using one-center integrals for the exchange (SOMF-1X) are also assessed here. Each time, only one of the terms was approximated while keeping the rest of the parameters as in our TBE. The results can be found in Figure 2 and Table S6.

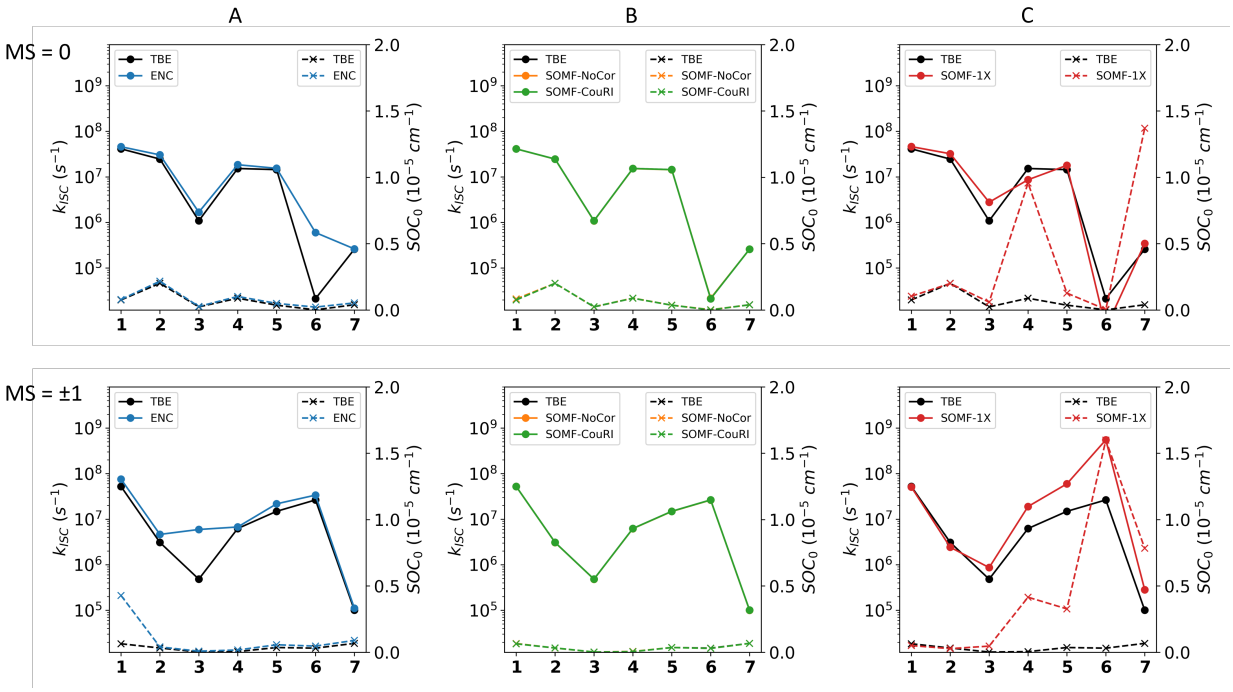

Figure 2. Comparison of the ISC rate values (full line, left axis) and zeroth-order SOCs (dashed line, right axis) for different SO Hamiltonians: Effective Nuclear Charge (ENC), exclusion of correlation (SOMF-NoCor), using the RI approximation for the Coulomb term (SOMF-Cou-RI), using one-center integrals for the exchange term (SOMF-1X), and our theoretical best estimate (TBE). Top (bottom) panel shows the values for MS=0 (MS=+1, having same values as MS=-1). In panel B, all the models are completely overlapping. SCS-ADC(2)/def2-TZVP//TDA-PBE0/6-311G(d,p) calculations with the AH, FC+HT, Cartesian vibronic model using a 10 cm^{-1} Lorentzian broadening.

When comparing the computed k_{ISC} values using the ENC approach and the TBE, only **3** (MS=±1) and **6** (MS=0) have a large difference (a factor of 12 and 28 resp.), while the average difference for the other compounds is 24% only. To further investigate the origin of the different errors, the purely electronic SOCs (first term in Eq. (11)) were also compared, see Figure 2A. First, it is interesting to note that for **1** (MS=±1), a large error in the SOC does not translate into a large error in the computed ISC rate. This is encouraging, since it shows that when taking the derivative, systematic errors can cancel out. The opposite happens in **3** and **6**, which only have a small difference in the SOC leading to significant changes in their rates. However, the electronic SOCs in these cases are rather small compared to the other compounds (*e.g.*, 8.3×10^{-8} cm^{-1} for **3**, see Table S7).

To better interpret these cases, we identified the normal modes leading to larger vibrational SOCs. The ΔSOC values (see Eq. (12)) for the normal mode displacements are shown in Figures 3 and S2. We underline that the largest contributions are found for low-frequency out-of-plane modes. This is similar to the HT effect for radiative transitions of symmetric molecules, where the decrease in symmetry leads to a dipole-allowed transition.[30] In contrast, the normal modes with a high Huang-Rhys factor (high vibronic coupling between electronic states) are mostly high-frequency modes (Figure S3). Focusing now on the problematic cases in the ENC model, namely **3** (MS = ±1) and **6** (MS = 0), one can see that the differences in the SOCs are much smaller than in **1**, again showing that the rate is sensitive to small errors in the SOCs.

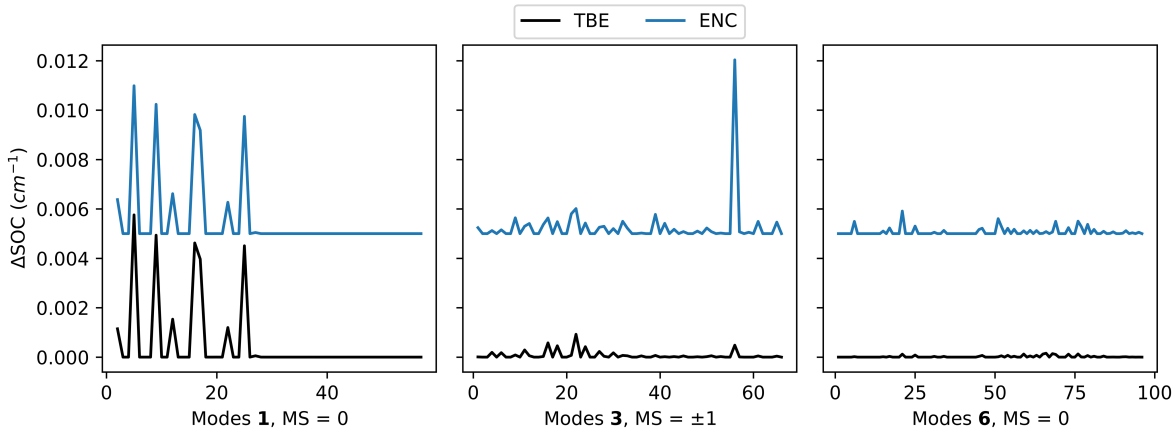

*Figure 3. ΔSOC for the displacement of the normal modes during the calculation of the SOC derivatives for each normal mode of **1** (MS = 0), **3** (MS = ±1), and **6** (MS = 0). The Effective Nuclear Charge (ENC) model (blue, shifted by 0.005 cm^{-1}) is compared with the theoretical best estimate (TBE). TDA-PBE0/6-311G(d,p) calculations.*

However, for some cases this behavior is not observed, since for example **4** (MS=±1) has a SOC of 5×10^{-8} (2×10^{-7}) cm^{-1} with the TBE (ENC) approach, while the difference in k_{ISC} is negligible. Thus, it seems that numerical artifacts can potentially strongly impact the results when the SOCs are small and it is advisable to treat the results carefully if ENC and TBE approaches yield significant differences.

Next, we discuss the differences within the chosen SOMF approaches. In Figure 2B one observes that neglecting the local correlation terms (SOMF-NoCor) has a negligible effect on the computed SOC matrix elements and thereto in the k_{ISC} values, which is consistent with the findings of Neese and coworkers.[38] A similar conclusion is found for the effect of using the RI approximation to calculate the Coulomb terms (SOMF-CouRI), which gives a maximum absolute error of 0.007% on k_{ISC}. In this case, small errors in the SOC translate to small errors in the rates. However, when using one- instead of four-center integrals for the exchange term (SOMF-1X), a divergence of several orders of magnitude on the computed k_{ISC} values compared to the TBE is observed. For instance, in **6** (MS=±1), there are large differences in both the computed SOCs (a factor of 51), and the k_{ISC} (a factor of 21). This approximation is the default method in ORCA 5.0, although in view of the present results for our series of compounds, we thus generally advise to carefully test the chosen SOMF approach to be used in k_{ISC} calculations, especially when the SOCs are small.

4.4. FQYs: Influence of the XCF

The selection of an appropriate XCF is certainly a challenge in TD-DFT, especially to correctly predict accurate energies or relative energies of states of different nature. Because of this, our calculations below always rely on the use of SCS-ADC(2)/def2-TZVP energies computed on top of the respective TDA-XCF/6-311G(d,p) optimized geometries. Therefore, the focus is set on assessing the performances of different functionals for the quality of the optimized geometries, Hessian matrices, and associated couplings. As mentioned above, five different XCFs including both global and range-separated hybrids with various admixture of *exact* exchange have been used (*i.e.*, B3LYP, PBE0, M06-2X, CAM-B3LYP, and ωB97X-D).

We start to evaluate the influence of the XCF on the radiative rates. Table 1 lists the experimental radiative rates, while the calculated rates are summarized in Table S8. Figure 4 shows a comparison between the computed k_r values obtained with various XCF and the experimental ones. All XCFs give similar results for the k_r, with a mean percentage error (MPE[†]) of 7% with respect to each other. As seen from the linear determination coefficient (R^2) values, calculated and measured rates are highly correlated. Furthermore, the maximum absolute error with respect to experiment is 0.35 for the logarithm of the rate (first point in Figure 4), but this corresponds to **3**, which also has the highest experimental variability ($\log(k_r) = 6.4$ - 7.3). These trends are consistent with the ones from our recent work.[17] Therefore, and regardless of the chosen XCF, the calculation of the radiative rates is sufficiently curated and thus, the possible errors in the FQY calculations should mainly originate from the estimates of the non-radiative rates.

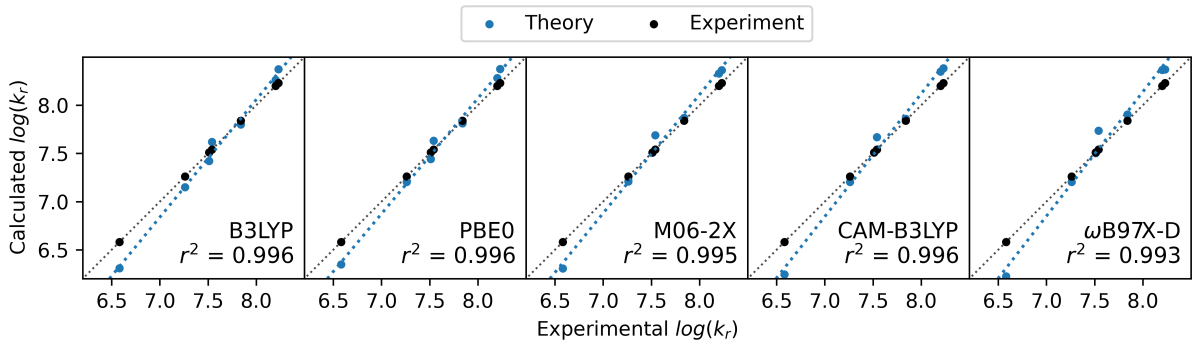

Figure 4. Calculated (black) versus average experimental (blue) logarithm of the fluorescence rate for different functionals. The r^2 value is calculated with a least-square linear fit (blue dotted line). SCS-ADC(2)/def2-TZVP//TDA-PBE0/6-311G(d,p) calculations with the AH, FC+HT, Cartesian vibronic model using a 10 cm^{-1} Lorentzian broadening.

Finally, we evaluate the influence of the XCF on the computed ISC rates for the $S_1 \rightarrow T_2$ channel and, therefore, their influence on the FQY values. The TBE approach detailed in the previous Section was used to determine the SOCs and ISC rates. Table S8 collects the numerical results for

[†] Calculated according to $MPE = \frac{1}{7*5}\sum_{j=1}^{7}\sum_{i=1}^{5}\frac{\left|x_i^j - \bar{x}_i\right|}{\bar{x}_i}$, with $\bar{x}_i$ the average calculated rate for XCF i.

the k_{ISC} values of **1**-**7** obtained with the different XCFs. There are not too large variations within the set of XCFs, although the MPE of 29% is significantly larger than for the fluorescence rates. The ISC rate is therefore slightly more sensitive than its radiative counterpart to the selected XCF.

We omit the comparison of the ISC rates with experiment because of the high experimental error on those values, but instead, we go directly to the comparison of FYQs. Figure 5 shows the computed FQYs. All XCFs tend to overestimate the experimental FQYs and there is a (weak, but clear) correlation between the calculated and experimental yields. Theory is able to explain ca. 70% of the experimental variability in the molecular set, though to our surprise, M06-2X seems to behave less accurately than the other XCFs in the present case. Furthermore, the MPE within the calculated results is 9% only, showing that the variability from the ISC rates is partially cancelled out when calculating FQYs. Interestingly, theory is quite good at pointing out the brightest and poorest emitters but does not provide accurate absolute values for the intermediate cases. A similar outcome was reported before for a series of fluoroborate dyes.[67] Certainly, the compounds possessing smaller FQYs are more prone to yield large deviations (see region below experimental FQY of 0.5 in Figure 5) because of *i*) the presence of an additional non-radiative channel (*e.g.*, IC), or *ii*) the accumulation and combination of errors potentially have a larger impact than in compounds possessing very large FQYs. In addition, the experimental values for compounds with intermediate FQYs values also show some degree of variability, see *e.g.*, in Table 1 the FQY values for phenanthrene (0.10 - 0.24) and/or anthracene (0.22 - 0.36).

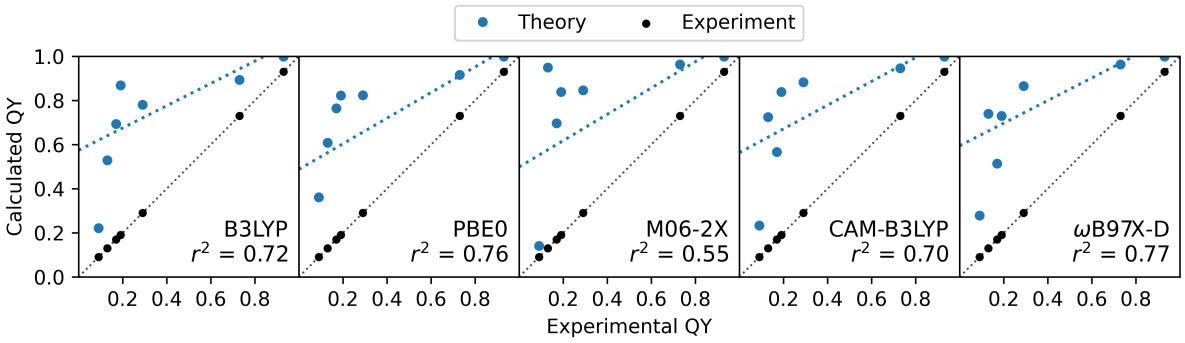

Figure 5. Calculated (black) versus average experimental (blue) FQYs for different functionals. SCS-ADC(2)/def2-TZVP//TDA-PBE0/6-311G(d,p) calculations with the AH, FC+HT, Cartesian vibronic model using a 10 cm^{-1} Lorentzian broadening.

4.5. Additional challenges for accurate FQYs

In order to shed some light into the above aspects, let us first further explore tetracene (**4**). For **4,** there is some experimental evidence that the $S_1 \rightarrow S_0$ IC channel is significantly involved in the total non-radiative decay. When including the $S_1 \rightarrow S_0$ IC rate derived experimentally by Wilkinson[23] and John B. Birks[19] (2×10^7 s^{-1}) in our kinetic models, we indeed see that the predicted FQYs fall within the experimental range (see Table 4).

*Table 4. FQY values (unity) calculated according Eq. (2) for **4**, with and without including the experimental IC rate $2*10^7$ s^{-1}. (SCS-ADC(2)/def2-TZVP//TDA-PBE0/6-311G(d,p), AH, FC+HT, Cartesian vibronic model using a 10 cm^{-1} Lorentzian broadening)*

	B3LYP	PBE0	M06-2X	CAM-B3LYP	ωB97X-D	Exp
No IC	0.87	0.82	0.84	0.82	0.73	0.16 - 0.21
$+IC_{exp}$	0.26	0.23	0.21	0.22	0.15	

Compounds **1** and **2** do not have any reliable experimental IC-ISC separation, so technically, a non-negligible part of their decay can also be IC. However, the theoretical errors for **3**, **5**-**7** cannot be explained by the neglect of a putative IC process since experimental evidence suggests that the non-radiative decay is 100% ISC.[16,21] A different source of error would be the calculated energies used for the decay rates. In a rough approximation, the radiative rate depends on the cube of the fluorescence energy, while non-radiative rates decrease exponentially with increasing energy (*e.g.*,

the energy gap between S_1-S_0 and S_1-T_x for IC and ISC, respectively). Thus even the rather small errors expected at SCS-ADC(2) level, ca. 0.2 eV, can have a larger impact on the rates. We therefore computed energies at CC3 level for **5** at the S_1 and T_2 minimum geometries to verify this (see Table S5 and Section S5 of the SI for computational details and data). The CC3 S_1-S_0 energy gap is smaller, while the S_1-T_2 gap is slightly larger than their SCS-ADC(2) counterparts, decreasing the fluorescence rate and increasing the ISC rate, as we are still in the normal Marcus region, where the energy gap law does not apply. Thereby, the FQY value for **5** lowers from 0.82 to 0.71, somewhat closer to the experimental value of 0.22-0.36, but a large deviation obviously pertains. As CC3 S-T gaps are likely very accurate, one can conclude that even though accurate energies do matter, the combination of errors from the frequencies, couplings, and vibronic models can still give a large deviation. Under these circumstances, we believe we have pushed the static strategy as much as possible: further improvements for rigid molecules would likely require a proper description of anharmonic effects, which is computationally much more demanding. Recent efforts in this direction include the use of Morse potentials instead of harmonic oscillators.[65] More approximated alternatives include the use of one-effective mode Marcus-Jortner-Levich models, which also use relevant quantities in the model computed at the minimal energy crossing points.[68]

5. Conclusions

We have presented a comprehensive and exhaustive investigation on the calculation of FQYs for a series of seven organic molecular systems. This study complements our recent efforts to benchmark many electronic structure and vibronic parameters for the calculation of the radiative rates.[17] Here we extend these initial efforts to the calculation of non-radiative rates, and especially the ISC rates, which is the predominant non-radiative decay channel for the herein investigated molecules. Specifically, we tested the impact of *i*) the electronic structure (chosen exchange-

correlation functional and SO Hamiltonian), and *ii*) the vibronic parameters (coordinate system, broadening function, and dipole expansion) for the ISC rate calculations. While the coordinate system and the broadening have minor impact on the calculated ISC rates, the chosen dipole expansion is critical because the ISC processes in these molecules is fully driven by the HT terms. The choice of the SO Hamiltonian can also have a large impact in the ISC calculations, especially when the purely electronic SOC contribution vanishes. Generally, for any arbitrary molecule we here advise to carefully test the available SOMF approaches. Concerning the chosen XCF, all XCFs tend to overestimate the experimental FQY values but the mean percentage error for the computed FQY values is 9% only. Thereby, we show that the variability arising from the chosen XCF for the optimized geometries, Hessian matrices, and associated couplings is relatively small. However, in agreement with our previous investigations, the influence of XCF is critical to correctly predict accurate energies or relative energies of states of different nature. Therefore, our calculations always rely on the use of SCS-ADC(2) energies. For a selected system, *i.e.*, anthracene (**5**), we use even more accurate CC3 energies. Although this helps getting closer to the measurement, it does not fully explain the deviation with respect to the experiment. Likely, as we demonstrate here for **4**, the neglect of alternative non-radiative channels besides ISC but also the combination of errors from the frequencies, couplings, and vibronic models, are likely behind the observed deviations. Further improvements to generalize FQY calculations would likely require going beyond the harmonic oscillator model, which is shown to be especially critical for the calculations of the IC rates.

ASSOCIATED CONTENT

Supporting Information.

The supporting information contains the following data: Tables with all relevant energies and excited state decay rates. Computational details of the CC3 calculations. Spin-orbit coupling differences and reorganization energies per mode for all compounds. An extensive explanation of the FQY simulation algorithm.

AUTHOR INFORMATION

Corresponding Author

*Daniel Escudero. E-mail: Daniel.escudero@kuleuven.be

Author Contributions

K. V.: Conceptualization, Investigation, Calculations, Formal analysis, Writing, Reviewing and Editing. M.H.E.B.: Conceptualization, Investigation. D.J.: Conceptualization, Investigation, Calculations, Formal analysis, Reviewing and Editing. D. E.: Conceptualization, Formal analysis, Writing, Reviewing and Editing, Funding acquisition. All authors have given approval to the final version of the manuscript.

Funding Sources

M.H.E.B and D.J. thank the CCIPL/Glicid computational center for generous allocation of computational time. D.E. acknowledges KU Leuven internal funds and FWO (project numbers G079122N and G0E5321N). The collaboration between the Nantes and Leuven teams was supported by the PHC program QCQY.

ACKNOWLEDGMENT

M.H.E.B and D.J. thank the CCIPL/Glicid computational center for generous allocation of computational time. D.E. acknowledges KU Leuven internal funds and FWO (project numbers G079122N and G0E5321N). The collaboration between the Nantes and Leuven teams was supported by the PHC program QCQY.

REFERENCES

(1) Kasha, M. Characterization of Electronic Transitions in Complex Molecules. *Discuss. Faraday Soc*. **1950**, *9* (c), 14. https://doi.org/10.1039/df9500900014.

(2) Kasha–Vavilov Rule. In *The IUPAC Compendium of Chemical Terminology*; International Union of Pure and Applied Chemistry (IUPAC): Research Triangle Park, NC, 2014. https://doi.org/10.1351/goldbook.K03371.

(3) Strickler, S. J.; Berg, R. A. Relationship between Absorption Intensity and Fluorescence Lifetime of Molecules. *J. Chem. Phys*. **1962**, *37* (4), 814–822. https://doi.org/10.1063/1.1733166.

(4) Kln, P.; Wirz, J. A Crash Course in Photophysics and a Classification of Primary Photoreactions. In *Photochemistry of Organic Compounds*; John Wiley & Sons, Ltd: Chichester, UK, 2009; pp 25–72. https://doi.org/10.1002/9781444300017.ch2.

(5) Ju, C.-W.; Bai, H.; Li, B.; Liu, R. Machine Learning Enables Highly Accurate Predictions of Photophysical Properties of Organic Fluorescent Materials: Emission Wavelengths and Quantum Yields. *J. Chem. Inf. Model*. **2021**, *61* (3), 1053–1065. https://doi.org/10.1021/acs.jcim.0c01203.

(6) Pérez-Escribano, M.; Jankowska, J.; Granucci, G.; Escudero, D. The Radiative Surface Hopping (RSH) Algorithm: Capturing Fluorescence Events in Molecular Systems within a Semi-Classical Non-Adiabatic Molecular Dynamics Framework. *J. Chem. Phys*. **2023**, *158* (12), 124104. https://doi.org/10.1063/5.0139516.

(7) de Souza, B.; Neese, F.; Izsák, R. On the Theoretical Prediction of Fluorescence Rates from First Principles Using the Path Integral Approach. *J. Chem. Phys*. **2018**, *148* (3), 034104. https://doi.org/10.1063/1.5010895.

(8) Niu, Y.; Peng, Q.; Deng, C.; Gao, X.; Shuai, Z. Theory of Excited State Decays and Optical Spectra: Application to Polyatomic Molecules. *J. Phys. Chem. A* **2010**, *114* (30), 7817–7831. https://doi.org/10.1021/jp101568f.

(9) Cerezo, J.; Santoro, F. FCclasses3 : Vibrationally-resolved Spectra Simulated at the Edge of the Harmonic Approximation. *J. Comput. Chem*. **2023**, *44* (4), 626–643.

https://doi.org/10.1002/jcc.27027.

(10) Veys, K.; Escudero, D. Computational Protocol To Predict Anti-Kasha Emissions: The Case of Azulene Derivatives. *J. Phys. Chem. A* **2020**, *124* (36), 7228–7237. https://doi.org/10.1021/acs.jpca.0c05205.

(11) Petrusevich, E. F.; Bousquet, M. H. E.; Ośmiałowski, B.; Jacquemin, D.; Luis, J. M.; Zaleśny, R. Cost-Effective Simulations of Vibrationally-Resolved Absorption Spectra of Fluorophores with Machine-Learning-Based Inhomogeneous Broadening. *J. Chem. Theory Comput.* **2023**, *19* (8), 2304–2315. https://doi.org/10.1021/acs.jctc.2c01285.

(12) Shuai, Z. Thermal Vibration Correlation Function Formalism for Molecular Excited State Decay Rates. *Chinese J. Chem.* **2020**, *38* (11), 1223–1232. https://doi.org/10.1002/cjoc.202000226.

(13) Ou, Q.; Peng, Q.; Shuai, Z. Toward Quantitative Prediction of Fluorescence Quantum Efficiency by Combining Direct Vibrational Conversion and Surface Crossing: BODIPYs as an Example. *J. Phys. Chem. Lett.* **2020**, *11* (18), 7790–7797. https://doi.org/10.1021/acs.jpclett.0c02054.

(14) Humeniuk, A.; Bužančić, M.; Hoche, J.; Cerezo, J.; Mitrić, R.; Santoro, F.; Bonačić-Koutecký, V. Predicting Fluorescence Quantum Yields for Molecules in Solution: A Critical Assessment of the Harmonic Approximation and the Choice of the Lineshape Function. *J. Chem. Phys.* **2020**, *152* (5), 054107. https://doi.org/10.1063/1.5143212.

(15) Manian, A.; Hudson, R. J.; Ramkissoon, P.; Smith, T. A.; Russo, S. P. Interexcited State Photophysics I: Benchmarking Density Functionals for Computing Nonadiabatic Couplings and Internal Conversion Rate Constants. *J. Chem. Theory Comput.* **2023**, *19* (1), 271–292. https://doi.org/10.1021/acs.jctc.2c00888.

(16) Stevens, B.; Algar, B. E. Intersystem Crossing Yields in Anthanthrene and Perylene from Photosensitised Peroxidation. *Chem. Phys. Lett.* **1967**, *1* (5), 219–220. https://doi.org/10.1016/0009-2614(67)85055-3.

(17) Bousquet, M. H. E.; Papineau, T. V.; Veys, K.; Escudero, D.; Jacquemin, D. Extensive Analysis of the Parameters Influencing Radiative Rates Obtained Through Vibronic Calculations. *J. Chem. Theory Comput.* **2023**, *in revisio*.

(18) Berlman, I. B. GRAPHS. In *Handbook of Fluorescence Spectra of Aromatic Molecules*; Elsevier, 1971; pp 107–415. https://doi.org/10.1016/B978-0-12-092656-5.50011-3.

(19) Birks, J. B. *Photophysics of Aromatic Molecules*, 1st ed.; Birks, J. B., Ed.; WILEY MONOGRAPHS IN CHEMICAL PHYSICS, 1970.

(20) Nijegorodov, N.; Mabbs, R.; Winkoun, D. . Influence of Weak and Strong Donor Groups on the Fluorescence Parameters and the Intersystem Crossing Rate Constant. *Spectrochim. Acta Part A Mol. Biomol. Spectrosc.* **2003**, *59* (3), 595–606. https://doi.org/10.1016/S1386-1425(02)00207-X.

(21) Horrocks, A. R.; Wilkinson, F. Triplet State Formation Efficiencies of Aromatic

Hydrocarbons in Solution. *Proc. R. Soc. London. Ser. A. Math. Phys. Sci.* **1968**, *306* (1485), 257–273. https://doi.org/10.1098/rspa.1968.0149.

(22) Van Haver, P.; Helsen, N.; Depaemelaere, S.; Van der Auweraer, M.; De Schryver, F. C. The Influence of Solvent Polarity of the Nonradiative Decay of Exciplexes. *J. Am. Chem. Soc.* **1991**, *113* (18), 6849–6857. https://doi.org/10.1021/ja00018a021.

(23) Kearvell, A.; Wilkinson, F. Internal Conversion from the Lowest Excited Singlet States of Aromatic Hydrocarbons. *Chem. Phys. Lett.* **1971**, *11* (4), 472–473. https://doi.org/10.1016/0009-2614(71)80387-1.

(24) Köhler, A.; Bässler, H. *Electronic Processes in Organic Semiconductors*; Wiley-VCH Verlag GmbH & Co. KGaA: Weinheim, Germany, **2015**. https://doi.org/10.1002/9783527685172.

(25) Shuai, Z.; Peng, Q. Excited States Structure and Processes: Understanding Organic Light-Emitting Diodes at the Molecular Level. *Phys. Rep.* **2014**, *537* (4), 123–156. https://doi.org/10.1016/j.physrep.2013.12.002.

(26) Veys, K.; Escudero, D. Anti-Kasha Fluorescence in Molecular Entities: Central Role of Electron–Vibrational Coupling. *Acc. Chem. Res.* **2022**, *55* (18), 2698–2707. https://doi.org/10.1021/acs.accounts.2c00453.

(27) F. Santoro, FCclasses: A Fortran 77 Code; 2008. (Available via the Internet at Http://Www.Pi.Iccom.Cnr.It/Fcclasses; Last Accessed 09/04/2021).

(28) Neese, F. The ORCA Program System. *Wiley Interdiscip. Rev. Comput. Mol. Sci.* **2012**, *2* (1), 73–78. https://doi.org/10.1002/wcms.81.

(29) Niu, Y.; Li, W.; Peng, Q.; Geng, H.; Yi, Y.; Wang, L.; Nan, G.; Wang, D.; Shuai, Z. MOlecular MAterials Property Prediction Package (MOMAP) 1.0: A Software Package for Predicting the Luminescent Properties and Mobility of Organic Functional Materials. *Mol. Phys.* **2018**, *116* (7–8), 1078–1090. https://doi.org/10.1080/00268976.2017.1402966.

(30) Herzberg, G.; Teller, E. Schwingungsstruktur Der Elektronenübergänge Bei Mehratomigen Molekülen. *Zeitschrift für Phys. Chemie* **1933**, *21B* (1), 410–446. https://doi.org/10.1515/zpch-1933-2136.

(31) Santoro, F.; Improta, R.; Lami, A.; Bloino, J.; Barone, V. Effective Method to Compute Franck-Condon Integrals for Optical Spectra of Large Molecules in Solution. *J. Chem. Phys.* **2007**, *126* (8), 084509. https://doi.org/10.1063/1.2437197.

(32) Santoro, F.; Improta, R.; Lami, A.; Bloino, J.; Barone, V. Erratum: "Effective Method to Compute Franck-Condon Integrals for Optical Spectra of Large Molecules in Solution" [J. Chem. Phys. 126, 084509 (2007)]. *J. Chem. Phys.* **2007**, *126* (16), 169903. https://doi.org/10.1063/1.2722259.

(33) Valiev, R. R.; Cherepanov, V. N.; Nasibullin, R. T.; Sundholm, D.; Kurten, T. Calculating Rate Constants for Intersystem Crossing and Internal Conversion in the Franck–Condon and Herzberg–Teller Approximations. *Phys. Chem. Chem. Phys.* **2019**, *21* (34), 18495–

18500. https://doi.org/10.1039/C9CP03183A.

(34) Penfold, T. J.; Gindensperger, E.; Daniel, C.; Marian, C. M. Spin-Vibronic Mechanism for Intersystem Crossing. *Chem. Rev.* **2018**, *118* (15), 6975–7025. https://doi.org/10.1021/acs.chemrev.7b00617.

(35) Marian, C. M. Spin-Orbit Coupling and Intersystem Crossing in Molecules. *Wiley Interdiscip. Rev. Comput. Mol. Sci.* **2012**, *2* (2), 187–203. https://doi.org/10.1002/wcms.83.

(36) Tatchen, J.; Gilka, N.; Marian, C. M. Intersystem Crossing Driven by Vibronic Spin–Orbit Coupling: A Case Study on Psoralen. *Phys. Chem. Chem. Phys.* **2007**, *9* (38), 5209. https://doi.org/10.1039/b706410a.

(37) Schimmelpfennig, B. AMFI: Atomic Spin–Orbit Integral Program. University of Stockholm 1996.

(38) Neese, F. Efficient and Accurate Approximations to the Molecular Spin-Orbit Coupling Operator and Their Use in Molecular g-Tensor Calculations. *J. Chem. Phys.* **2005**, *122* (3), 034107. https://doi.org/10.1063/1.1829047.

(39) Shao, Y.; Head-Gordon, M. An Improved J Matrix Engine for Density Functional Theory Calculations. *Chem. Phys. Lett.* **2000**, *323* (5–6), 425–433. https://doi.org/10.1016/S0009-2614(00)00524-8.

(40) Malkin, J. *Photophysical and Photochemical Properties of Aromatic Compounds*, illustrate.; CRC Press, 1992, 1992.

(41) Salahub, D. R.; Zerner, M. C. ChemInform Abstract: The Challenge of d and f Electrons. Theory and Computation. *ChemInform* **1990**, *21* (33). https://doi.org/10.1002/chin.199033368.

(42) Hohenberg, P.; Kohn, W. Inhomogeneous Electron Gas. *Phys. Rev.* **1964**. https://doi.org/10.1103/PhysRev.136.B864.

(43) Kohn, W.; Sham, L. J. Self-Consistent Equations Including Exchange and Correlation Effects. *Phys. Rev.* **1965**. https://doi.org/10.1103/PhysRev.140.A1133.

(44) Casida, M. E. Time-Dependent Density Functional Response Theory for Molecules; 1995; pp 155–192. https://doi.org/10.1142/9789812830586_0005.

(45) Runge, E.; Gross, E. K. U. Density-Functional Theory for Time-Dependent Systems. *Phys. Rev. Lett.* **1984**, *52* (12), 997–1000. https://doi.org/10.1103/PhysRevLett.52.997.

(46) Hirata, S.; Head-Gordon, M. Time-Dependent Density Functional Theory within the Tamm–Dancoff Approximation. *Chem. Phys. Lett.* **1999**, *314* (3–4), 291–299. https://doi.org/10.1016/S0009-2614(99)01149-5.

(47) Becke, A. D. Density-functional Thermochemistry. III. The Role of Exact Exchange. *J. Chem. Phys.* **1993**, *98* (7), 5648–5652. https://doi.org/10.1063/1.464913.

(48) Adamo, C.; Barone, V. Toward Reliable Density Functional Methods without Adjustable Parameters: The PBE0 Model. *J. Chem. Phys.* **1999**. https://doi.org/10.1063/1.478522.

(49) Zhao, Y.; Truhlar, D. G. The M06 Suite of Density Functionals for Main Group Thermochemistry, Thermochemical Kinetics, Noncovalent Interactions, Excited States, and Transition Elements: Two New Functionals and Systematic Testing of Four M06-Class Functionals and 12 Other Function. *Theor. Chem. Acc.* **2008**, *120* (1–3), 215–241. https://doi.org/10.1007/s00214-007-0310-x.

(50) Yanai, T.; Tew, D. P.; Handy, N. C. A New Hybrid Exchange–Correlation Functional Using the Coulomb-Attenuating Method (CAM-B3LYP). *Chem. Phys. Lett.* **2004**, *393* (1–3), 51–57. https://doi.org/10.1016/j.cplett.2004.06.011.

(51) Chai, J.-D.; Head-Gordon, M. Long-Range Corrected Hybrid Density Functionals with Damped Atom–Atom Dispersion Corrections. *Phys. Chem. Chem. Phys.* **2008**, *10* (44), 6615. https://doi.org/10.1039/b810189b.

(52) Frisch G. W.; Schlegel, H. B.; Scuseria, G. E.; Robb, M. A.; Cheeseman, J. R.; Scalmani, G.; Barone, V.; Petersson, G. A.; Nakatsuji, H.; Li, X.; Caricato, M.; Marenich, A. V.; Bloino, J.; Janesko, B. G.; Gomperts, R.; Mennucci, B.; Hratch, D. J., M. J. . T. Gaussian 16, Rev. A.03. *Gaussian, Inc., Wallingford, CT* **2016**. https://doi.org/111.

(53) Shao, Y.; Gan, Z.; Epifanovsky, E.; Gilbert, A. T. B.; Wormit, M.; Kussmann, J.; Lange, A. W.; Behn, A.; Deng, J.; Feng, X.; Ghosh, D.; Goldey, M.; Horn, P. R.; Jacobson, L. D.; Kaliman, I.; Khaliullin, R. Z.; Kuś, T.; Landau, A.; Liu, J.; Proynov, E. I.; Rhee, Y. M.; Richard, R. M.; Rohrdanz, M. A.; Steele, R. P.; Sundstrom, E. J.; Woodcock, H. L.; Zimmerman, P. M.; Zuev, D.; Albrecht, B.; Alguire, E.; Austin, B.; Beran, G. J. O.; Bernard, Y. A.; Berquist, E.; Brandhorst, K.; Bravaya, K. B.; Brown, S. T.; Casanova, D.; Chang, C.-M.; Chen, Y.; Chien, S. H.; Closser, K. D.; Crittenden, D. L.; Diedenhofen, M.; DiStasio, R. A.; Do, H.; Dutoi, A. D.; Edgar, R. G.; Fatehi, S.; Fusti-Molnar, L.; Ghysels, A.; Golubeva-Zadorozhnaya, A.; Gomes, J.; Hanson-Heine, M. W. D.; Harbach, P. H. P.; Hauser, A. W.; Hohenstein, E. G.; Holden, Z. C.; Jagau, T.-C.; Ji, H.; Kaduk, B.; Khistyaev, K.; Kim, J.; Kim, J.; King, R. A.; Klunzinger, P.; Kosenkov, D.; Kowalczyk, T.; Krauter, C. M.; Lao, K. U.; Laurent, A. D.; Lawler, K. V.; Levchenko, S. V.; Lin, C. Y.; Liu, F.; Livshits, E.; Lochan, R. C.; Luenser, A.; Manohar, P.; Manzer, S. F.; Mao, S.-P.; Mardirossian, N.; Marenich, A. V.; Maurer, S. A.; Mayhall, N. J.; Neuscamman, E.; Oana, C. M.; Olivares-Amaya, R.; O'Neill, D. P.; Parkhill, J. A.; Perrine, T. M.; Peverati, R.; Prociuk, A.; Rehn, D. R.; Rosta, E.; Russ, N. J.; Sharada, S. M.; Sharma, S.; Small, D. W.; Sodt, A.; Stein, T.; Stück, D.; Su, Y.-C.; Thom, A. J. W.; Tsuchimochi, T.; Vanovschi, V.; Vogt, L.; Vydrov, O.; Wang, T.; Watson, M. A.; Wenzel, J.; White, A.; Williams, C. F.; Yang, J.; Yeganeh, S.; Yost, S. R.; You, Z.-Q.; Zhang, I. Y.; Zhang, X.; Zhao, Y.; Brooks, B. R.; Chan, G. K. L.; Chipman, D. M.; Cramer, C. J.; Goddard, W. A.; Gordon, M. S.; Hehre, W. J.; Klamt, A.; Schaefer, H. F.; Schmidt, M. W.; Sherrill, C. D.; Truhlar, D. G.; Warshel, A.; Xu, X.; Aspuru-Guzik, A.; Baer, R.; Bell, A. T.; Besley, N. A.; Chai, J.-D.; Dreuw, A.; Dunietz, B. D.; Furlani, T. R.; Gwaltney, S. R.; Hsu, C.-P.; Jung, Y.; Kong, J.; Lambrecht, D. S.; Liang, W.; Ochsenfeld, C.; Rassolov, V. A.; Slipchenko, L. V.; Subotnik, J. E.; Van Voorhis, T.; Herbert, J. M.; Krylov, A. I.; Gill, P. M. W.; Head-Gordon, M. Advances in Molecular Quantum Chemistry Contained in the Q-Chem 4 Program Package.

Mol. Phys. **2015**, *113* (2), 184–215. https://doi.org/10.1080/00268976.2014.952696.

(54) Ou, Q.; Bellchambers, G. D.; Furche, F.; Subotnik, J. E. First-Order Derivative Couplings between Excited States from Adiabatic TDDFT Response Theory. *J. Chem. Phys.* **2015**. https://doi.org/10.1063/1.4906941.

(55) Send, R.; Furche, F. First-Order Nonadiabatic Couplings from Time-Dependent Hybrid Density Functional Response Theory: Consistent Formalism, Implementation, and Performance. *J. Chem. Phys.* **2010**, *132* (4), 044107. https://doi.org/10.1063/1.3292571.

(56) Neese, F. Software Update: The ORCA Program System, Version 4.0. *Wiley Interdiscip. Rev. Comput. Mol. Sci.* **2018**, *8* (1). https://doi.org/10.1002/wcms.1327.

(57) Dreuw, A.; Wormit, M. The Algebraic Diagrammatic Construction Scheme for the Polarization Propagator for the Calculation of Excited States. *Wiley Interdiscip. Rev. Comput. Mol. Sci.* **2015**, *5* (1), 82–95. https://doi.org/10.1002/wcms.1206.

(58) Weigend, F.; Häser, M.; Patzelt, H.; Ahlrichs, R. RI-MP2: Optimized Auxiliary Basis Sets and Demonstration of Efficiency. *Chem. Phys. Lett.* **1998**, *294* (1–3), 143–152. https://doi.org/10.1016/S0009-2614(98)00862-8.

(59) Hellweg, A.; Grün, S. A.; Hättig, C. Benchmarking the Performance of Spin-Component Scaled CC2 in Ground and Electronically Excited States. *Phys. Chem. Chem. Phys.* **2008**, *10* (28), 4119. https://doi.org/10.1039/b803727b.

(60) TURBOMOLE V7.1 2016, a Development of University of Karlsruhe and Forschungszentrum Karlsruhe GmbH, 1989-2007, TURBOMOLE GmbH, since 2007; Available from Http://Www.Turbomole.Com.

(61) Duschinsky, F. The Importance of the Electron Spectrum in Multi Atomic Molecules. Concerning the Franck-Condon Principle. *Acta Physicochim. URSS* **1937**, *7*, 551–566.

(62) Avila Ferrer, F. J.; Santoro, F. Comparison of Vertical and Adiabatic Harmonic Approaches for the Calculation of the Vibrational Structure of Electronic Spectra. *Phys. Chem. Chem. Phys.* **2012**, *14* (39), 13549. https://doi.org/10.1039/c2cp41169e.

(63) Cerezo, J.; Santoro, F. Revisiting Vertical Models To Simulate the Line Shape of Electronic Spectra Adopting Cartesian and Internal Coordinates. *J. Chem. Theory Comput.* **2016**, *12* (10), 4970–4985. https://doi.org/10.1021/acs.jctc.6b00442.

(64) Cerezo, J.; Zúñiga, J.; Requena, A.; Ávila Ferrer, F. J.; Santoro, F. Harmonic Models in Cartesian and Internal Coordinates to Simulate the Absorption Spectra of Carotenoids at Finite Temperatures. *J. Chem. Theory Comput.* **2013**, *9* (11), 4947–4958. https://doi.org/10.1021/ct4005849.

(65) Valiev, R. R.; Merzlikin, B. S.; Nasibullin, R. T.; Kurtzevitch, A.; Cherepanov, V. N.; Ramazanov, R. R.; Sundholm, D.; Kurtén, T. Internal Conversion Rate Constant Calculations Considering Duschinsky, Anharmonic and Herzberg–Teller Effects. *Phys. Chem. Chem. Phys.* **2023**, *25* (8), 6406–6415. https://doi.org/10.1039/D2CP05275J.

(66) Wang, Y.; Ren, J.; Shuai, Z. Evaluating the Anharmonicity Contributions to the Molecular Excited State Internal Conversion Rates with Finite Temperature TD-DMRG. *J. Chem. Phys.* **2021**, *154* (21), 214109. https://doi.org/10.1063/5.0052804.

(67) Rybczyński, P.; Bousquet, M. H. E.; Kaczmarek-Kędziera, A.; Jędrzejewska, B.; Jacquemin, D.; Ośmiałowski, B. Controlling the Fluorescence Quantum Yields of Benzothiazole-Difluoroborates by Optimal Substitution. *Chem. Sci.* **2022**, *13* (45), 13347–13360. https://doi.org/10.1039/D2SC05044G.

(68) Bozzi, A. S.; Rocha, W. R. Calculation of Excited State Internal Conversion Rate Constant Using the One-Effective Mode Marcus-Jortner-Levich Theory. *J. Chem. Theory Comput.* **2023**, *19* (8), 2316–2326. https://doi.org/10.1021/acs.jctc.2c01288.